Technical Report

Signal to Noise Ratio (S/N) in DSI probes. The Consequences of Increased Sample Temperature on the S/N ratio in MAS Experiments.

By

George Entzminger and Paul Ellis

Problem Statement

Doty Scientific, Incorporated (DSI) is recognized as one of the major manufacturers of NMR probes in the area solid-state NMR spectroscopy. Typical applications of these probes would address fundamental problems in Chemistry, Materials Science, and Biology. Within the area of solid-state NMR probe development, DSI has two major competitors: Agilent (formerly Varian Associates) and Bruker. Both competitors have consistently reported *experimental* signal to noise (S/N) ratios as their figure of merit for their probes. However, both often do not report power levels and/or the corresponding $\pi/2$ pulse width. A consequence is the end user often has no idea of the efficiency of the probe making a comparison between vendors difficult. DSI on the other hand reports *predicted* power levels and $\pi/2$ pulse widths. The *predicted* power levels and pulse widths follow from extensive bench testing in combination with computer models for each probe type. This allows the end user to develop a feeling for the efficiency of the probe. However, such feelings or levels of trust are no substitute for hard *experimental* numbers.

To that end, this report will detail the determination of the S/N ratio and power levels for two standard DSI MAS probes: a 4 mm wide bore probe with a $BMAX_{XY}$ coil assembly on an XC4 stator and a narrow bore 3 mm Drop-In probe with a $BMAX_{XY}$ Coil on a DI3 stator. The basic coil topology for the $BMAX_{XY}$ design is a solenoid coil is wrapped about the appropriate stator with a DE (Doty-Entzminger) coil (a low E-field high frequency coil – usually tuned for ^1H) is wrapped around a solenoid coil. Henceforth, for the purposes of this report we will refer to these probes as the $BMAX_{XY}$-4 (4 mm probe with a $BMAX_{XY}$ coil assembly) and DI-3 (Drop-In 3 mm probe with a $BMAX_{XY}$ coil assembly), respectively. Both probes are double tuned and experiments were performed in a wide bore 11.75 T magnet.

No attempt was made in this report to use the highest possible power to yield the shortest pulse widths. We intentionally left 1 dB of attenuation on the ^1H amplifier, simply because none of the experiments we report here required the higher power levels.

Recall, that probe efficiency[1-3], η, aside from various geometrical factors, is inversely proportional to the incident power, P, in W, and the square of the 360° pulse width, τ_{360}, in s, i.e.

$$\eta \propto \left[\tau_{360}^2 \bullet P\right]^{-1}$$

Hence, a probe is more efficient the shorter the 360° pulse width is for a given power. An important corollary to probe efficiency is if the end user suspects a probe problem; always determine the $\pi/2$ pulse width for the probe. If the $\pi/2$ pulse width is the same as in previous measurements for a given power level, then the problem is *not* with the probe.

Approach

The approach taken here reflects what the end user would want in probe comparisons; S/N ratio, power levels, and pulse widths at *room temperature*. The latter point is important and takes account of the consequences of frictional heating, which occurs in MAS experiments. A corollary to these measurements is the determination of the temperature gradient the sample experiences in MAS experiments. Such numbers will be a welcome addition to rf-efficiencies reported for a given MAS probe.

The first phase of this effort will be the determination of the temperature of the sample as a function of MAS speed for a fixed bearing pressure. The air-bearing[4] utilized in modern MAS probe designs is the principle origin of the temperature increase in MAS experiments. Current MAS spinning speed controllers alter and control the air bearing and drive gas pressures for a given spinning speed. To avoid the situation where the air bearing pressure changes from one spinning speed to another we simply fixed the pressure. In the present case we selected ~45 psi as the air-bearing (inlet) pressure. The spinning and bearing gas was boil-off N_2 and no attempt beyond normal pressure regulation at the wall was utilized in these experiments.

To measure the sample temperature during MAS experiments we used the standard $Pb(NO_3)_2$ experiments. This approach was first utilized by Bielecki and Burum[5] and subsequently refined by several groups.[6-12] For purposes of our work we utilized a calibration factor of 0.7117 ppm/°C as reported in the Supplemental Information found of reference 12.

In the original paper Bielecki and Burum[5] made an incisive observation that was subsequently followed by Dybowski and coworkers[13]; namely the ^{207}Pb shielding tensor for Pb site in $Pb(NO_3)_2$ was changing as function of temperature. Stated simply, the structure (unit cell parameters, and perhaps motion within the unit cell) was changing as a function of the temperature and these effects are responsible for observed temperature dependence of the ^{207}Pb chemical shift. That being the case, it suggests *pressure* would also influence the ^{207}Pb chemical shift. We will report on the consequences of pressure on the observed chemical shift in a different report. However, it is evident that in a MAS experiment the pressure experienced by Pb-isochromate depends on its radial location within the sample. As a result ^{207}Pb NMR may be good thermometer, but a poor choice for the determination of the temperature distribution with a sample undergoing fast spinning. As a consequence of sensitivity of ^{207}Pb resonance to pressure, the temperature gradient that we report here represents an upper limit to the gradient.

The $BMAX_{xy}$-4 Probe

The ^{207}Pb power level and $\pi/2$ pulse width were 235W and 4.12 μs, respectively. Typically, we utilized a 1 μs pulse width for the experiments performed in the

determination of the sample temperature. To avoid any issues associated with laboratory temperature variation (for example the consequences of HVAC cycling), we controlled the probe temperature to 27 °C. This value was defined to be the temperature of the sample in the absence of sample spinning.

The stator and rotor for the 4 mm probe were made of Si_3N_4. The end caps (long) were made from glass filled Torlon® and were 7.01 mm in length. The length of the rotor was 20.95 mm. The sample occupied the central 6.93 mm of the rotor. The air-bearing holes (12) are 1.7 mm from either end of the rotor. The basic idea is to cool the air-bearing gas to offset the temperature increase induced by the friction between the stator and the rotor. Typically, Doty probes are supplied with independent heaters for both the drive and bearing gas streams, allowing independent control of the temperature of either gas stream. The special conditions used here didn't take advantage of this feature. In our experiments the cooling gas utilized in the variable temperature (VT) experiments is the bearing gas and whatever temperature gradient that develops across the sample in the MAS experiment may not necessarily be alleviated in VT experiments. Cooling the drive gas would only have minimal effects on the observed gradient across the sample. We utilized the standard DSI VT set-up using liquid N_2 as the cooling medium and a dual set of half-turn coils (only one of the coils was utilized – the bearing coil) that provided the "contact" between the coolant and the VT/bearing gas. With the sample temperature changes expected (a few 10s of °C) in these experiments, the liquid N_2 and the single half-coil provided sufficient cooling power. The temperature was regulated with a DSI Probe Temperature Controller to ±0.1 °C.

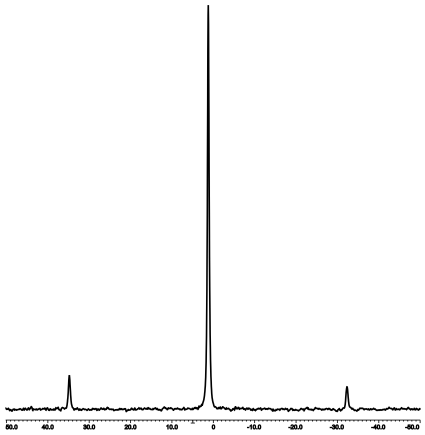

Figure 1

As an illustration of the S/N ratio in the ^{207}Pb experiments the Figure 1 presents the results of using four π/2 pulses a 90 s delay between pulses at a spinning speed of 3.5 kHz. The S/N ratio (~300:1) is excellent and typically we utilized a single pulse in our experiments. A summary of the raw data for the $BMAX_{xy}$-4 probe (showing increased temperature relative to room temperature for a given spinning speed) is summarized in Table 1 and plotted in Figure 2.

Table 1
Relative Temperature Increase with Spinning Speed
For the $BMAX_{xy}$-4 Probe

Spinning Speed (kHz)	Temperature Increase (°C)
1.5	0
3.5	1.50
5.5	4.03
7.5	8.32
9.5	14.24
11.5	22.37
13.5	32.83
15.5	45.03

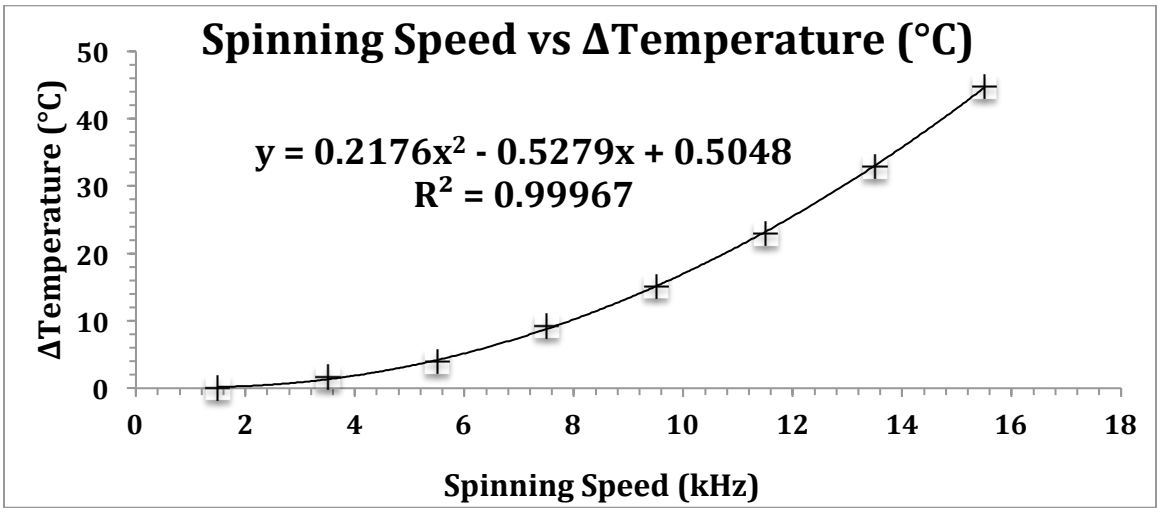

Figure 2

The Si_3N_4 stator/rotor combination can be spun up to 24 kHz. Due to the density of the $Pb(NO_3)_2$ sample, we limited the spinning speed to 15.5 kHz in these experiments. While spinning at 1.5 kHz, we assumed the temperature of the sample was essentially the same as room temperature. All subsequent temperatures were expressed relative the sample temperature spinning at 1.5 kHz. The temperature dependence as a function of spinning speed was easily fit to a quadratic polynomial. The highest temperature the sample experiences relative to room temperature was 45.03 °C while spinning at 15.5 kHz. Such a temperature increase is typical for stator/rotor combinations of this size. All other factors being equal, the larger the stator/rotor combination the higher the temperature. Likewise, for a given stator/rotor combination the higher the spinning speed the higher the temperature becomes.

Using the quadratic polynomial, summarized in Figure 2, we can extrapolate beyond the highest spinning speed we determined (15.5 kHz) to predict the sample temperature while spinning at 17.5, 19.5, and 21.5 kHz. Those temperatures are 57.90, 72.95, and 89.74 °C, respectively. Recall, these temperatures are relative to room temperature; which in this case 27 °C. The point is clear; spinning at high speeds can yield important spectroscopic data. However, that data comes at a cost, i.e. increased sample temperature. It is essential to compensate for such a temperature increase during any high speed MAS experiment.

Recall the sample occupies the central 6.93 mm of the rotor (or ± 3.46 mm with respect to the center of the rotor). As the spinning speed is increased (even at 1.5 kHz) the lineshape becomes asymmetric. The asymmetry in the lineshape has the appearance of axially symmetric powder pattern (convoluted with a right triangle); yet the magic angle has not changed.[14] Continuing this analogy, the perpendicular edge is deshielded with respect to the parallel edge. Due to the consequences of pressure on the lineshape, we will focus our attention of the asymmetry that exists at the half-height linewidth. To examine the asymmetry in more detail we divided the lineshape into two halves (relative to the maximum in the lineshape). For example the 1.5 kHz half-height line width had a "left half" width of 0.191 ppm and a "right half" width of 0.214 ppm. To make the analysis of the lineshapes easier we assume that "right half" width is more reflective of the temperature gradient. Hence, the asymmetry reported in Table 2 is simply twice the left half width subtracted from the total linewidth. The symmetric width would be 0.382 ppm and the asymmetric width at 1.5 kHz would be 0.030 ppm or 0.04 °C. To make the gradients relative to 1.5 kHz data we simply subtracted the symmetric widths from the remaining data. The assumption being that these symmetric widths (at 1.5 kHz) are more reflective of magnetic field inhomogeneity than temperature affects. These data are summarized in Table 2. This asymmetry is easy to observe due to the sensitivity of the ^{207}Pb chemical shift to temperature.

Table 2

Estimated Temperature Gradients Across the Rotor Relative to Spinning at 1.5 kHz for the BMAX$_{xy}$-4 Probe

Spinning Speed (kHz)	Asymmetry Half Height[a]	ΔT(°C)Half Height
1.5[b]	0.030	0.04
3.5	0.030	0.04
5.5	0.05	0.07
7.5	0.2	0.3
9.5	0.4	0.6
11.5	0.5	0.8
13.5	0.8	1.1
15.5	1.0	1.5

Footnotes for Table 2

a. Units are in ppm.
b. Symmetric Half Height line width was 0.382 ppm.

In all cases where an asymmetry existed, the dominant gradient was to higher shielding (cooler than ensemble reflecting the temperature of resonance maximum). At the highest spinning speed the temperature gradient as reflected in the half height line width is modest and is 1.5 °C. The temperature gradient becomes worse as the spinning speed increases. When the temperature was decreased for the highest spinning speed the gradient did not decrease (data not shown). The asymmetry in the case of ^{13}C resonances (which are less sensitive to temperature changes) would be less apparent, but the temperature gradients still persist.

$BMAX_{xy}$-4 Probe S/N Ratio for Glycine and HMB. We characterized the ^{13}C performance of the $BMAX_{xy}$-4 probe by examining the S/N ratio of a sample of α-glycine (49.7 mg or 662.08 μmoles)[15] and that of HMB (37.9 mg or 233.56 μmoles) . All of the normal CP[16,17] parameters were optimized on each sample. For α-glycine: relaxation delay (20 s), contact time (7.5 ms) with a ramped[18] CP (0%), ^{1}H π/2 pulse width of (2.8 μs), and the TPPM phase angle (15.5°). Likewise, for HMB: relaxation delay 20 s, contact time 4 ms, with CW decoupling, ^{1}H π/2 pulse width of (2.8 μs), and a ramped CP (11%). The power utilized for decoupling in both experiments was the same, i.e. 199 W. During the spin-lock the power on the ^{1}H side was 97.4 W, while on the ^{13}C side 93.1 W. These powers correspond to a $\gamma B_1/2\pi$ of 62.4 kHz. Each sample was spun and controlled at 10 kHz (±2 Hz). In the case of α-glycine the spectrum was the result of 4 accumulations; the S/N ratio was 189:1 while for HMB a single shot was utilized resulting in a S/N of 199:1. Using the graph depicted within Figure 2 we reduced the temperature of the sample by 15 °C and retuned the probe. While characterizing the temperature dependence using $Pb(NO_3)_2$ we checked that reducing the temperature by 15 °C returned the sample back to room temperature. To within a degree or 2, the sample was back to room temperature. The accuracy of the returning back to a given temperature depends on several factors and as a result the end users needs to calibrate this adjustment.

The ^{13}C side of the probe had changed its tuning such that we re-optimized the power for CP. We repeated the experiment keeping the remaining NMR parameters fixed at their previous values. The resulting S/N ratio for α-glycine was 205:1 and for HMB the S/N ratio was 232:1. In each case we utilized the JEOL RMS Window S/N calculation. For glycine the noise region was the best 15 ppm in the range from -10 to -70 ppm and the signal window was 60 to 10 ppm. In the case of HMB the noise region was the best 15 ppm in the range from -80 to -130 ppm and the signal window was 30 to 5 ppm. The spectra, not compensated for the temperature increase due to MAS experiment and compensated for the temperature increase, for α-glycine are depicted in Figures 3 and 4, respectively while those for HMB are illustrated in Figures 5 and 6, respectively.

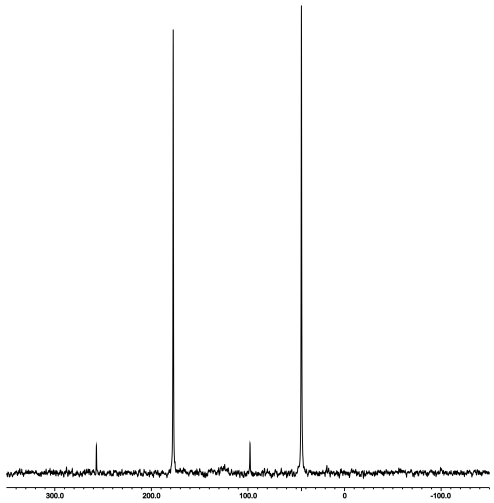

Figure 3

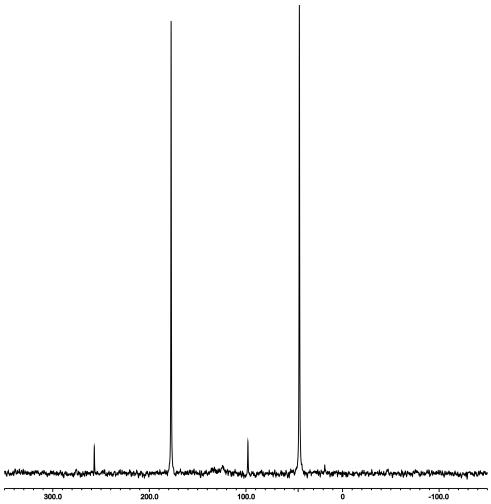

Figure 4

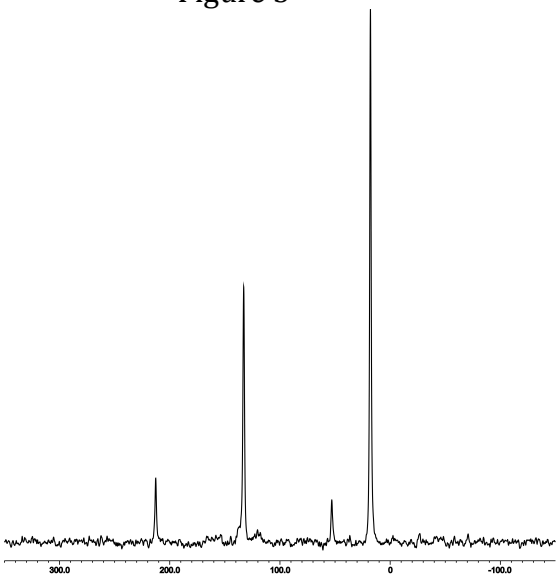

Figure 5

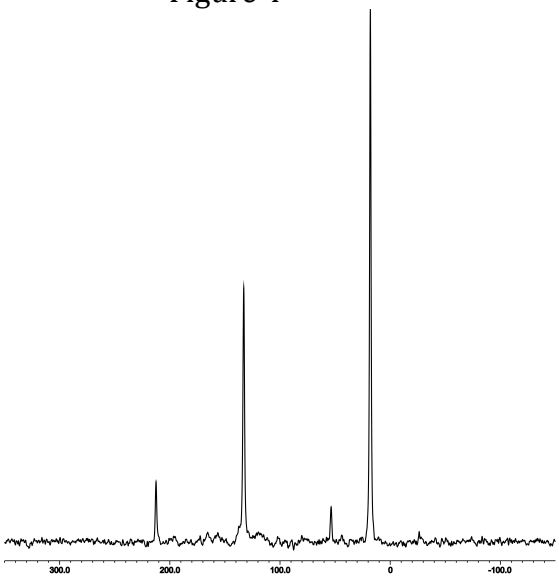

Figure 6

Using 199 W we obtained a ^{1}H $\pi/2$ pulse width of 2.8 μs or a $\gamma B_1/2\pi$ of 89.2 kHz. However, we utilized 97.5 W during the ^{1}H spinlock, or $\gamma B_1/2\pi$ of 62.4 kHz. Under CP conditions we obtained the same $\gamma B_1/2\pi$ with only 93 W for ^{13}C. These data are summarized in Table 3. Current specifications for the $BMAX_{xy}$-4 probe are 85 kHz at 278 W for protons. Clearly, our experimental data is slightly better than the specifications and as a result the predicted performance of the probe is in keeping with experiment.

As an internal check on our S/N ratio measurements and an indirect determination of the error in those measurements we can utilize the glycine results to predict the results for HMB at a given temperature. Converting the glycine number to a single scan the S/N ratio would be 102:1. That S/N arose from 662.08 μmoles of the CH_2 carbon within glycine. Taking the ratio of the number of μmoles for the two samples and then correcting for the six equivalent carbons in HMB, the predicted S/N for

HMB at room temperature is 216:1. Experimentally we found 232:1. Comparing the two numbers provides an estimate of the relative error in these measurements.

Table 3
Summary of Probe Performance

	$BMAX_{xy}$-4	DI-3
^{1}H Power (W)	199	199
π/2 (μs)	2.8	3.0
^{1}H Power (W)[a]	97.4	97.5
$\gamma B_1/2\pi$ (^{1}H kHz)[a]	62.4	58.5
^{13}C Power (W)[a]	93.1	53.0
S/N (α-Glycine)[b]	205:1	103:1
μmoles of α-Glycine	662.08	291.74
S/N (HMB)	232:1[c]	129:1[d]
μmoles of HMB	233.56	108.46
ΔT_{Max} (°C)	1.5[e]	1.0[f]

Footnotes for Table 3.

a. Under spin-lock conditions.

b. Spinning at 10 kHz (±2 Hz), 4 accumulations with a 20 s delay between pulses, with a contact time of 7.5 ms at room temperature.

c. Spinning 10 kHz (±2 Hz), 1 accumulation with a 20 s delay, and a 4 ms contact at room temperature.

d. Spinning 10 kHz (±2 Hz), 4 accumulations were acquired, however, we divided that S/N ratio by a factor of 2 to obtain the equivalent single scan S/N ratio, with a 20 s delay, and a 4 ms contact at room temperature.

e. The spinning speed was 15.5 kHz (±2 Hz). The "gradient" was measured at the half-height linewidth relative to spinning at 1.5 kHz. See text for details.

f. The spinning speed was 21.5 kHz (±2 Hz). The "gradient" was measured at the half-height linewidth relative to spinning at 1.5 kHz. See text for details.

The DI-3 Probe

The DI3 probe we utilized for this work is a prototype narrow bore version. Perhaps what is not obvious at this point is what does "Drop In" or "DI" mean in the context of this probe? Within the NMR community there is a certain degree of convenience associated with changing the sample in an MAS experiment. The "old-fashioned" approach was is to drop the probe from the magnet, open the probe body, and replace the sample, then put the probe back together, put probe back into the magnet and retune. A more convenient approach is simply to "eject" the sample and drop a new sample into the probe, and then retune. From the perspective of the present report, the design difference between the DI-3 probe as opposed to the

$BMAX_{xy}$-4 probe is the airflow characteristics associated with the stator/rotor assembly. The coil assemblies for both probes are similar. Do these design differences have significant impact on sample heating during an MAS experiment? Before we can address this question, we again have to perform a series of $Pb(NO_3)_2$ experiments.

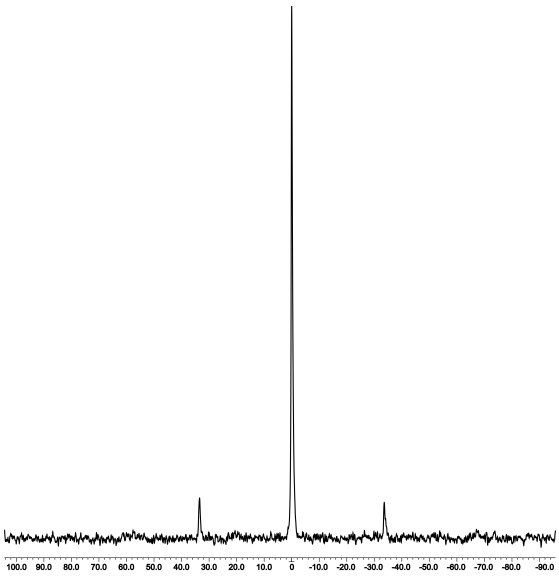

Figure 7

A typical ^{207}Pb NMR experiment on $Pb(NO_3)_2$ for the DI-3 is shown in Figure 7. The S/N ratio is 130:1. This spectrum is the result of 1 shot with $\pi/2$ pulse width of 3.18 μs using 196 W while spinning at 3.5 kHz. As before, we set and controlled the temperature of the probe (in the absence of spinning) to 27 °C. To be consistent with the previous set of experiments, we selected ~45 psi as the air-bearing (inlet) pressure. In experiments where we employed slower spinning speeds (1.5 to 7.5 kHz) we used a drive pressure of 11 psi and a bearing pressure of 20 psi. This latter condition will lead to a small discontinuity in the temperature *vs.* spinning speed plot. In the remaining higher spinning speed experiments the drive and bearing pressures were increased to 36 psi and 45 psi, respectively. This was necessary due to the spinning efficiency of the DI-3. As before we have collected a series of ^{207}Pb NMR experiments as a function of spinning speed and translated the change in chemical shift into a temperature difference. The $Pb(NO_3)_2$ sample had a "packed" density of ~2.7 g/mL. For safety reasons we did not spin this sample beyond 21.5 kHz. These data are summarized in Table 4 and graphically depicted in Figure 8.

Using the quadratic polynomial, summarized in Figure 8, we can extrapolate beyond the highest spinning speed we determined (21.5 kHz) to predict the sample temperature while spinning at 23.5, 25.5, 27.5, 29.5 and 31.5 kHz. Those temperatures are 52.99, 63.40, 74.76, 87.07, and 100.31 °C, respectively. Recall, these temperatures are relative to room temperature; which in this case 27 °C. Even

with the smaller diameter stator/rotor it is essential to compensate for such a temperature increase during any high speed MAS experiment.

Table 4
Relative Temperature Increase with Spinning Speed
For the DI-3 Probe

Spinning Speed (kHz)	Temperature Increase (°C)
1.5	0
3.5	0.73
5.5	2.34
7.5	4.99
9.5	5.93
11.5	9.84
13.5	14.71
15.5	20.70
17.5	27.38
19.5	34.72
21.5	44.00

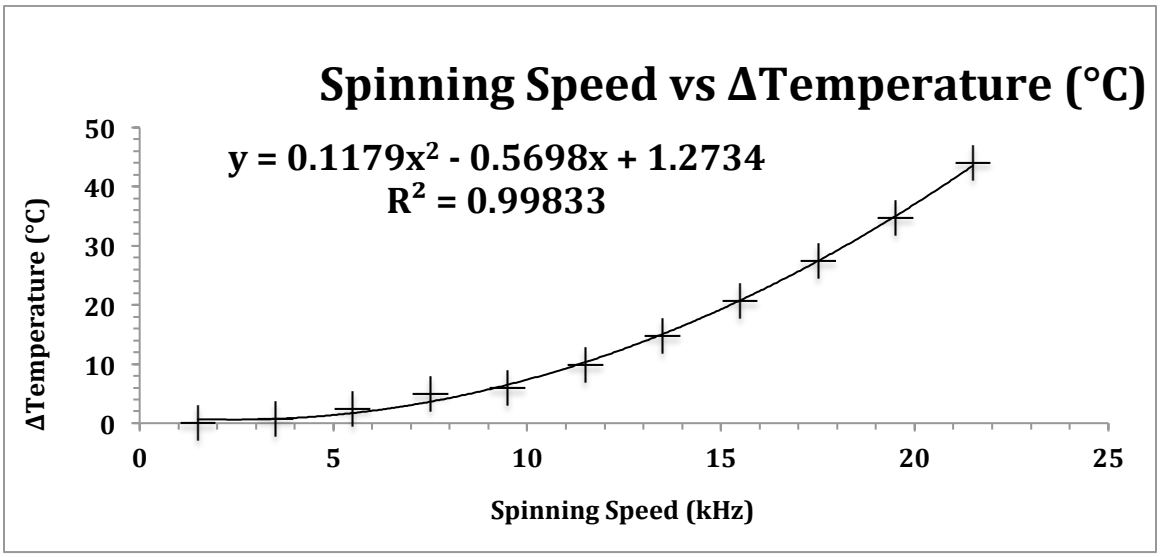

Figure 8

The spinning speed for the DI-3 probe can be easily fit to a quadratic polynomial. The maximum temperature the sample experiences is 44.0 °C (or relative to room temperature is 27.0 °C) at the highest spinning speed (21.5 kHz).

As we did previously we estimated the gradient experienced by the sample was estimated by examining the lineshape at the half height linewidth. Like the 4 mm probe, the DI-3 also had an asymmetry at all spinning speeds. To be consistent with

the results summarized in Table 2 we divided the lineshape into two halves (relative to the maximum in the lineshape). For example the 1.5 kHz half-height line width had a "left half" width of 0.2014 ppm and a "right half" width of 0.2678 ppm. To make the analysis of the lineshapes easier we assume that "right half" width is more reflective of the temperature gradient. Hence, the asymmetry reported in Table 5 is simply is twice the left hand width subtracted from the total linewidth. The symmetric width would be 0.4028 ppm and the asymmetric width at 1.5 kHz would be 0.066 ppm or 0.09 °C. To make the gradients relative to 1.5 kHz data we simply subtracted the symmetric widths from the remaining data. The assumption being that these symmetric widths (at 1.5 kHz) are more reflective of magnetic field inhomogeneity than temperature affects. These data are summarized in Table 5.

Table 5

Estimated Temperature Gradients Across the Rotor Relative to Spinning at 1.5 kHz for the DI-3 Probe

Spinning Speed (kHz)	Asymmetry Half Height[a]	ΔT(°C)Half Height
1.5[b]	0.066	0.09
3.5	0.068	0.07
5.5	0.090	0.13
7.5	0.217	0.31
9.5	0.145	0.20
11.5	0.212	0.30
13.5	0.258	0.36
15.5	0.338	0.48
17.5	0.434	0.61
19.5	0.557	0.78
21.5	0.759	1.07

Footnotes for Table 5

a. Units are in ppm.

b. The symmetric half height line width was 0.4028 ppm.

DI-3 Probe S/N Ratio for Glycine and HMB. We characterized the ^{13}C performance of the DI-3 probe by examining the S/N ratio of a sample of α-glycine (21.9 mg or 291.74 μmoles) and HMB (17.6 mg or 108.46 μmoles). The sample was centered within the coil and occupied the central 6 mm. We used the same decoupling and contact time, etc. as we utilized for the $BMAX_{xy}$-4 probe. The only difference was due to the temperature correction. The temperature correction for spinning at 10 kHz for the DI-3 was on the order of 5 °C and as such we felt it was too small to correct. In the case of α-glycine the spectrum was the result of 4 accumulations; the S/N ratio was 103:1. Using the same number of accumulations for HMB a S/N of 258:1 was obtained. The resulting spectra for α-glycine and HMB

are plotted in Figures 9 and 10, respectively. The performance details for the DI-3 are summarized in Table 3.

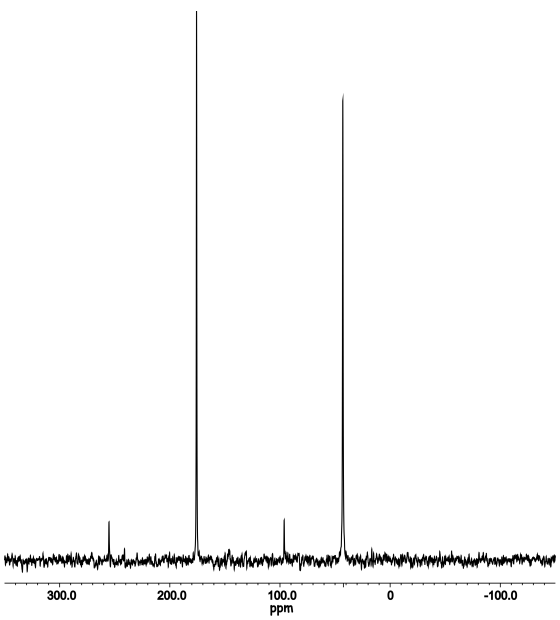

Figure 9

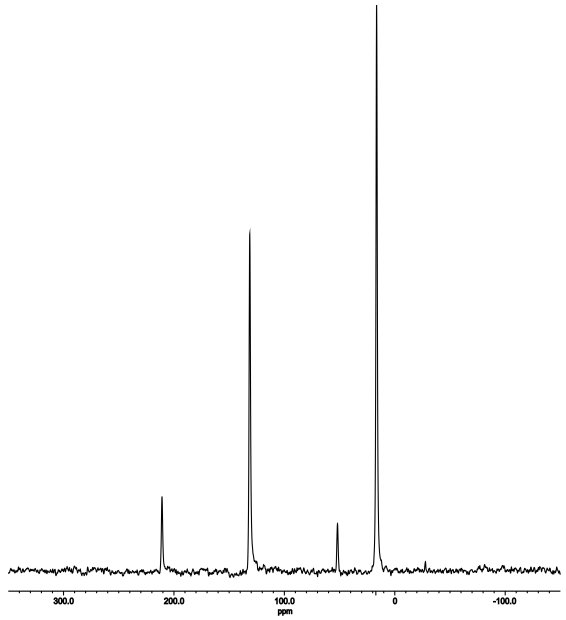

Figure 10

As an internal check on our S/N ratio measurements and an indirect determination of the error in those measurements we can utilize the glycine results to predict the results for HMB at a given temperature. The glycine S/N arose from 291.74 μmoles of the CH_2 carbon within glycine. Taking the ratio of the number of μmoles for the two samples and then correcting for the six equivalent carbons in HMB, the predicted S/N for HMB at room temperature is 230:1. Experimentally we found 258:1. As before, comparing the two numbers provides an estimate of the relative error in these measurements.

Summary and Conclusions

The performance specification for the $BMAX_{xy}$-4 and the DI-3 are summarized with Table 3. Recall the coil configurations between the two probes are the same. The main difference is the airflow over the rotor. During the course of these efforts we wanted to examine the temperature gradient at the 15% point in the lineshape. The results obtained did not make sense, if we just considered the lineshape being affected by simply temperature. After some thought and additional experiments we realized there that the 15% point in the ^{207}Pb NMR lineshape of $Pb(NO_3)_2$ is heavily affected by the radial pressure gradient that exists within the rotor. We will report on these experiments in a different report. It is clear, ^{207}Pb NMR spectroscopy of $Pb(NO_3)_2$ represents an excellent thermometer. However, if interest lies in the temperature distribution within the sample, more work is needed to clarify the role of pressure has on the ^{207}Pb lineshape under rapid magic angle spinning.

The performance for both probes (S/N ratio, $\pi/2$ pulse widths for a given power level) was excellent. Neither probe showed any tendency towards arcing at the power levels employed. Spinning speed and temperature are easily set and show the desired stability over long time intervals. From the data acquired it is essential to compensate for the increased temperature induced by the high speed spinning.

Acknowledgements

The authors wish to express our gratitude for the continuing support of Dr. David Doty and the many helpful comments and suggestions he has made during the course of this effort. Likewise, the authors wish to express their appreciation to Messrs. Jerry Hacker and Marc Bremmer for their valuable technical assistance with our experiments. The authors further want to express there gratitude to JB Spitzmesser for his machining of the $Pb(NO_3)_2$ cells used in conjunction with the $BMAX_{xy}$-4 experiments and Scott Deese for the discussions relative to stator designs.

References

(1) Doty, F. D.; Inners, R. R.; Ellis, P. D. *J. Magn. Reson.* **1981**, *43*, 399.
(2) Doty, F. D., Connick, T. J., Ni, X. Z., and Cligan, M. N. *J. Magn. Reson* **1988**, *77*, 536.
(3) Stringer, J. A.; Drobny, G. P. *Rev. Sci. Instrum.* **1998**, *69*, 3384.
(4) Doty, F. D.; Ellis, P. D. *Rev. Sci. Instrum.* **1981**, *52*, 1868.
(5) Bielecki, A.; Burum, D. P. *Journal of Magnetic Resonance, Series A* **1995**, *116*, 215.
(6) Ferguson, D. B.; Haw, J. F. *Anal. Chem.* **1995**, *67*, 3342.
(7) van Gorkom, L. C. M.; Hook, J. M.; Logan, M. B.; Hanna, J. V.; Wasylishen, R. E. *Magn. Reson. Chem.* **1995**, *33*, 791.
(8) Neue, G.; Dybowski, C. *Solid State Nucl. Magn. Reson.* **1997**, *7*, 333.
(9) Takahashi, T.; Kawashima, H.; Sugisawa, H.; Toshihide, B. *Solid State Nucl. Magn. Reson.* **1999**, *15*, 119.
(10) Langer, B.; Schnell, I.; Spiess, H. W.; Grimmer, A.-R. *J. Magn. Reson.* **1999**, *138*, 182.
(11) Martin, R. W.; Zilm, K. W. *J. Magn. Reson.* **2004**, *168*, 202.
(12) Concistrè, M.; Gansmüller, A.; McLean, N.; Johannessen, O. G.; Marín Montesinos, I.; Bovee-Geurts, P. H. M.; Verdegem, P.; Lugtenburg, J.; Brown, R. C. D.; DeGrip, W. J.; Levitt, M. H. *J. Am. Chem. Soc.* **2008**, *130*, 10490.
(13) Dmitrenko, O.; Bai, S.; Beckmann, P. A.; van Bramer, S.; Vega, A. J.; Dybowski, C. *The Journal of Physical Chemistry A* **2008**, *112*, 3046.
(14) We independently verified this by using a laser and a small mirror. Within our experimental error (less than a millidegree), we were unable to detect any change in the magic angle as a function of spinning speed.
(15) Foerster, H., Struppe, J., Steuernagel, S., Aussenacc, F., Benivelli, F., Gierth, P. *Solid State NMR AVANCE Solids User Manual*; Bruker Biospin GmbH: Rheinstetten, Germany, 2008.
(16) Pines, A.; Gibby, M. G.; Waugh, J. S. *J. Chem. Phys.* **1972**, *56*, 1776.
(17) Pines, A.; Gibby, M. G.; Waugh, J. S. *Journal of Chemical Physics* **1973**, *59*, 569
(18) Metz, G.; Wu, X. L.; Smith, S. O. *Journal of Magnetic Resonance, Series A* **1994**, *110*, 219.